Renewable Energy 80 (2015) 205–218

Contents lists available at ScienceDirect

Renewable Energy

journal homepage: www.elsevier.com/locate/renene

A statistical methodology for the estimation of extreme wave conditions for offshore renewable applications

Xiaoli Guo Larsén [a, *], Christina Kalogeri [b], George Galanis [b, c], George Kallos [b]

[a] Technical University of Denmark, Risø Campus, Wind Energy Department, Roskilde, Denmark
[b] University of Athens, School of Physics, Division of Environmental Physics, Meteorology, Atmospheric Modeling and Weather Forecasting Group, University Campus, Bldg. PHYS-V, Athens, 15784, Greece
[c] Hellenic Naval Academy, Section of Mathematics, Xatzikyriakion, Piraeus, 18539, Greece

ARTICLE INFO

Article history:
Received 3 March 2014
Accepted 30 January 2015
Available online 25 February 2015

keywords:
Significant wave height
The 50-year return significant wave height
Spectral correction

ABSTRACT

Accurate estimation of extreme wave conditions is critical for offshore renewable energy activities and applications. The use of numerical wind and wave models gives a credible and convenient way of monitoring the general atmospheric and sea state conditions, especially in the absence of sufficient observational networks. However, when focusing on the study of non-frequent cases, in particular over coastal areas, increased uncertainty in the model outputs and accordingly in the reliability of the estimation of extreme waves becomes an important issue. The current study introduces a methodology to validate and post-process outputs from a high resolution numerical wave modeling system for extreme wave estimation based on the significant wave height. This approach is demonstrated through the data analysis at a relatively deep water site, FINO 1, as well as a relatively shallow water area, coastal site Horns Rev, which is located in the North Sea, west of Denmark. The post-processing targets at correcting the modeled time series of the significant wave height, in order to match the statistics of the corresponding measurements, including not only the conventional parameters such as the mean and standard deviation, but also a new parameter, the second-order spectral moment. This second-order spectral moment is essential for extreme value estimation but has so far been neglected in relevant studies. The improved model results are utilized for the estimation of the 50-year values of significant wave height as a characteristic index of extreme wave conditions. The results from the proposed methodology seem to be in a good agreement with the measurements at both the relatively deep, open water and the shallow, coastal water sites, providing a potentially useful tool for offshore renewable energy applications.

1. Introduction

Accurate estimation of the extreme wave height is essential for design of offshore and coastal structures such as wind turbines and platforms. Such an estimate requires long term, good quality measurements, which are seldom available.

To complement the shortage of measurements, long term, climatological outputs from wave models have been used for calculating the extreme wave atlas, e.g. Refs. [1,10,11,14,39,40,47].

However, the outputs from the existing wave models, even the most advanced ones as we will discuss in the following, are sometimes limited for the estimation of the extreme values. It is a common phenomenon and challenge that the smoothing effect as embedded in numerical modeling will lead to flattened variability at relatively high frequencies, resulting in the "missing peaks" as discussed extensively in the review article of [13]. In Ref. [13]; a thorough discussion was given on the challenges for wave modeling of storm conditions. One of the challenges lies in the limitation of existing mesoscale wave models in resolving the response of waves to the fast turbulent atmospheric forcing during strong wind conditions; together with the limitations of the atmospheric models in resolving the gust, this leads to "missing peaks" in the wave modeling. The modeling is even more challenging in the coastal areas.

The wave model (WAM) has been utilized in numerous studies, not only for deep waters but also for coastal areas and sheltered seas [14,39,40]. Note that in these studies, they validated the model through mean wave statistics rather than extreme values [5]. used

* Corresponding author. +45 2132 7332.
E-mail address: xgal@dtu.dk (X.G. Larsén).

http://dx.doi.org/10.1016/j.renene.2015.01.069
0960-1481/

WAM, and through H_s, they showed that the model captured the storm events at several sites in the North Sea with rather deep water, including FINO 1. The shallow water formulations incorporated in the latest WAM version make the model capable of simulating the wave conditions reaching performance comparable to the coastal models like SWAN applied in higher resolution [9]; although both WAM and SWAN need improvement for shallow waters in the coastal zones. It has been observed frequently that for shallow waters, the significant wave height, H_s, is over-predicted for strong wind conditions, both with WAM [14,25,39,40] and coastal models MIKE 21 SW and SWAN [48]. This reflects the challenges in wave modeling for issues of swell decay in the coastal zones.

Whereas forecast of waves has been performed at much higher horizontal resolution, such as 1–2 km in Ref. [41]; the existing extreme wave atlases were often made from data of coarser resolutions, e.g. those from the ERA-40 reanalysis correspond to a horizontal resolution of 1.5° [11]; those in Ref. [10] have a horizontal resolution of 0.125° and those in Ref. [1] 10 km. The data analyzed here, within the framework of the EU MARINA Platform project, are outputs from a new version of WAM run at a resolution of 5 km. The model has been endowed with routines that take into account of shallow water effects, which is expected to improve the simulation for the coastal areas. WAM, as well as the forcing atmospheric system SKIRON, was implanted with assimilation modules for correcting their initial conditions based on available wind and wave in situ and remote sensing records [15,17,23].

By reviewing the difficulties and uncertainties related to the current wave modeling systems, in this study, we aim at developing a statistical approach to implement missing information as in the modeled data through measurements.

In this study, first, it will be shown through the analysis of measurements that even with a high resolution of 5 km and with routines taking into account of shallow water effect, the most up-to-date model is limited in resolving the high frequency variability of H_s. This phenomenon, as examined through the literature, shows to be a general issue with wave modeling, even with SWAN at fine resolution. The impact of the high frequency variability on the extreme value estimation is shown here to be important through spectral moments (Section 4) and should not be neglected. None of the published studies regarding the extreme wave height have taken this into account.

In this study, we define the extreme wave height as the significant wave height, H_s, with a 50-year return period, denoted as H_s^{50}.

The paper is accordingly structured as follows. The measurements, including one open water, rather deep water and one coastal, rather shallow water site, are introduced in section 2. The wave model and the atmospheric model that provides the wind force to the wave model are described in section 3. Section 4 introduces the spectral correction method. In section 5, the use of two statistical methods for the estimation of the T-year return value, the periodic maximum method and the peak-over-threshold method, is described. Data analysis, the post-processing procedure and the results of H_s^{50} are presented in section 6, followed by discussions and conclusions in sections 7 and 8.

2. Measurements

The wave measurements used in this study are recorded at two offshore sites: Horns Rev and FINO 1. The locations of the two sites are shown in Fig. 1.

Horns Rev is a coastal site. The water depth at this site varies from 6 to 12 m. According to the distribution of the ratio of water depth (D) and the peak wave length (L_w), $r = D/L_w$, the site can be considered as intermediate to shallow water (Table 1). The wave

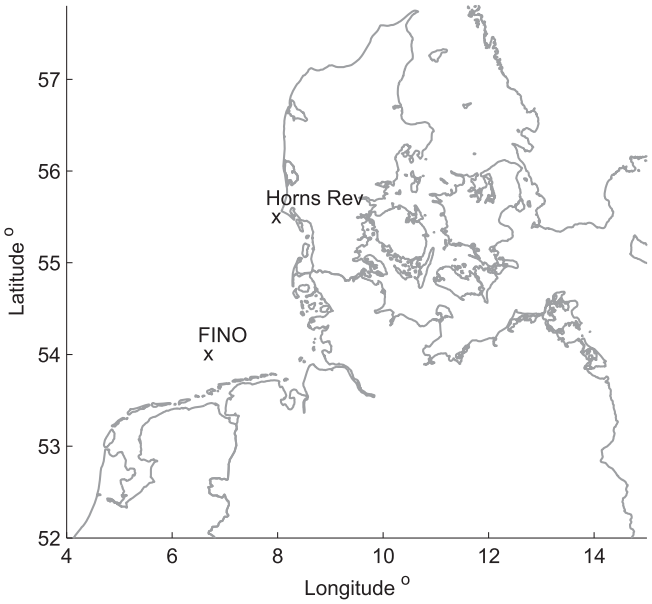

Fig. 1. Locations of the shallow water site Horns Rev and the deep water site FINO 1.

measurements were made through a Wave Rider buoy. The details of the measurements can be found in Refs. [43]; the buoy data used in the current study were from "Wave Rider S" as referred to in Ref. [43] (their Figs. 4–14). The waves were measured through the vertical acceleration of the buoy. As the buoy follows the waves, the force of the mooring line will change. The force is produced by the changing immersion of the buoy, resulting in an error of 1.5% maximum [46]. The significant wave height was derived from a 1D wave power spectrum measured by the buoy. The data are available from July 1999 to June 2006, half hourly. Data analysis was done in Ref. [43] for the year 2004 where the data quality was considered to be reliable. Similar data examination was done here for 1999 to 2006 and we did not find any abnormal data distribution behaviors and therefore conclude that the data quality is fine. The data coverage for each month from 2001 to 2006 is listed in Table 2. The information about the monthly data coverage is important when we need the spectrum from measurements for the spectral correction method proposed here in this study, which can only be calculated from continuous time series (see section 6.1).

FINO 1 has rather open ocean condition. The water depth is 30 m. According to the distribution of $r = D/L_w$, it can be considered as an intermediate to deep water site (Table 1). The wave measurements at FINO 1 analyzed in this paper were made from a directional waverider DWR (Datawell BV). The data quality was examined in terms of comparison with measurements from four other different instruments in Ref. [44]. The consistent statistics between the various measurements suggest a good data quality. More details about the measurements at FINO 1 can be found in Ref. [44]. The data used here are half hourly and are from 2003 to 2013. The data coverage is on average much less than the Horns Rev site and it is shown in Table 3 for each month.

Table 1
The distribution of the ratio between water depth and the peak wave length $r = D/L_w$ at the coastal site Horns Rev and open water site FINO 1.

Site	$r < \frac{1}{20}$ shallow	$r < \frac{1}{10}$	$r < \frac{1}{5}$	$\frac{1}{20} < r < \frac{1}{2}$ intermediate	$r > \frac{1}{2}$ deep
Horns Rev	0.8%	24.3%	76.4%	98.2%	1%
FINO 1	0%	0.8%	7.6%	57.3%	42.7%

Table 2
Data coverage (%) for each month from 2001 to 2006 for the buoy measured wave data at Horns Rev.

Month	2001	2002	2003	2004	2005	2006
Jan	49.7	89.7	85.8	98.2	95.3	59.3
Feb	0	86.8	88.5	84.1	95.4	43.8
Mar	0	90.2	97.6	70.8	99.7	27.1
Apr	0	98.6	95.2	70.8	95.3	49.3
May	0	94.0	98.9	99.9	99.2	67.0
Jun	21.0	97.6	98.5	99.5	76.0	73.5
Jul	45.2	97.8	98.1	99.9	99.5	0
Aug	48.6	94.4	95.8	99.9	75.2	0
Sep	54.4	99.5	90.9	92.9	97.6	0
Oct	91.6	94.1	97.4	94.6	87.0	0
Nov	99.7	97.5	43.4	82.4	86.3	0
Dec	93.3	71.3	99.9	96.8	72.3	0

3. The models

The wave model WAM [19,29] has been used here to simulate 10-year wave data. WAM is a third generation wave model that solves the wave transport equation explicitly without presumptions on the shape of the wave spectrum. It presents the physics of the wave evolution and uses a full set of degrees of freedom of a 2D wave spectrum. Here, the ECMWF (European Centre for Medium range Weather Forecasting) version, CY33R1 [7,22] has been employed. Compared to conventional use of WAM, a number of improvements have been adopted, including (1) the extension of the advection scheme in the wave energy balance equation to account for the corner points using the Corner Transport Upstream scheme, thus providing a more uniform propagation in all directions. (2) a new parameterization of shallow water effect that affects both the time evolution of the wave spectrum and the determination of the kurtosis of the wave field [24]. Detailed description of the shallow water features of WAM can also be found in, e.g. Refs. [6,8,35]. (3) technical modifications to define the minimum time step, which have been proven valuable for the use of the model in high resolution grids.

The WAM model domain covers the North Atlantic ($20^\circ N - 75^\circ N, 50^\circ W - 30^\circ E$) as shown in Fig. 2. The far west part of the domain is included to capture the important swell propagation. The model was run with a resolution of 0.05° by 0.05°. The wave spectrum is discretized into 25 frequencies ranging from 0.0417 to 0.5476 Hz and 24 equally spaced directions. The propagation time step is set to 75 s. For the current study, WAM has been driven by 3-hourly wind inputs. The wind inputs are wind speed and direction at 10 m from the atmospheric model SKIRON. The main output of the wave model is the distribution of wave energy $S_W(f,\theta)$ as a function of frequency (f) and direction (θ). The significant wave height H_s is the average of the largest one-third of wave heights (the difference in surface elevation between the wave crest and the wave trough) in an irregular sea-state and H_s is estimated based on the zero-order spectral moment of the wave spectrum: $H_{m_0} = 4\sqrt{\int_0^\infty S_W(f)df}$.

SKIRON is a modeling system developed at National and Kapodistrian University of Athens [26]. The model is based on the ETA/National Center for Environmental Prediction (NCEP) model, originally developed by Refs. [37] and [21]. In the model, the vertical turbulence mixing is performed by mixing coefficients of the modified Mellor-Yamada 2.5 level turbulence. In the surface layer, the Monin-Obukhov similary theory is used. The non-linear lateral diffusion scheme with the diffusion coefficient depending on the deformation and the turbulent kinetic energy is introduced in order to control the level of small-scale noises.

The SKIRON model domain is also shown in Fig. 2, with the same horizontal spatial resolution as WAM, with 45 vertical levels up to 50 hPa and a time step of 15 s. As initial conditions, the SKIRON model uses fields from a high-resolution (0.15°) regional reanalysis prepared with the implementation of Local Analysis and Prediction System (LAPS) assimilation system [3,4]. The initial guess fields are ECMWF 0.5° by 0.5° operational analysis fields. The lateral conditions are updated every 3 h. The model utilizes daily sea surface temperature (SST) fields from NCEP with a resolution of 0.5°. The model output of the wave parameters is recorded hourly.

It is worth noting that available observations from in-situ (meteorological stations and buoys) and remote sensing data (ENVISAT and TOPEX satellite records) for wind and wave parameters were assimilated into the atmospheric and wave models respectively by utilizing the standard assimilation schemes of SKIRON and WAM models [15,17,23,34]. Additional information for assimilation systems for atmospheric and wave models can be found in e.g. Refs. [27] and [42].

4. The spectral correction method

As introduced in section 1, modeled variables miss variability at high frequencies due to smoothing effect of the models, so that the small scale variabilities are unresolved. Fig. 3a shows such an example for FINO 1 where the power spectrum of the modeled H_s misses the energy for $f > 2 \cdot 10^{-5}$ Hz.

In Refs. [31]; it was shown through a Gaussian process that the impact from this missed energy on the calculation of extreme value can be quantified through the spectral moments. It was shown that the impact is considerable and should not be neglected. The spectral correction method was developed to fill in the missing variability of the modeled variable at high frequencies.

In Refs. [31]; it was assumed that the once-per-year exceedance F follows a Poisson process $F = \exp(-\lambda T_0)$, where T_0 is the period

Table 3
Data coverage (%) for each month from 2003 to 2013 for the buoy measured wave data at FINO 1.

Month	2003	2004	2005	2006	2007	2008	2009	2010	2011	2012	2013
Jan	0	90.0	47.2	92.7	47.1	99.9	48.5	0	36.2	100	100
Feb	0	63.1	96.3	16.6	35.5	99.8	41.7	12.1	99.9	100	100
Mar	0	19.2	54.8	0	8.1	99.7	36.6	52.2	100	99.8	100
Apr	0	43.7	99.9	32.3	45.0	100	45.3	25.3	28.4	100	100
May	0	94.1	100	99.9	41.5	49.9	20.6	49.2	96.0	99.9	0
Jun	0	87.0	99.7	99.9	49.2	24.1	40.0	62.4	99.9	100	0
Jul	0.2	0	100	84.6	48.3	50.0	72.1	68.1	99.9	57.8	0
Aug	0.3	84.4	99.6	73.1	45.8	50.0	49.7	72.6	100	34.5	0
Sep	0	38.8	30.2	99.9	45.8	20.8	0	76.8	100	100	0
Oct	69.8	0.1	100	99.9	4.3	43.5	35.5	77.8	100	99.1	0
Nov	66.7	0.3	100	51.5	23.8	46.6	56.4	73.3	100	100	0
Dec	46.3	47.6	99.9	46.8	100	49.3	0	74.9	99.9	100	0

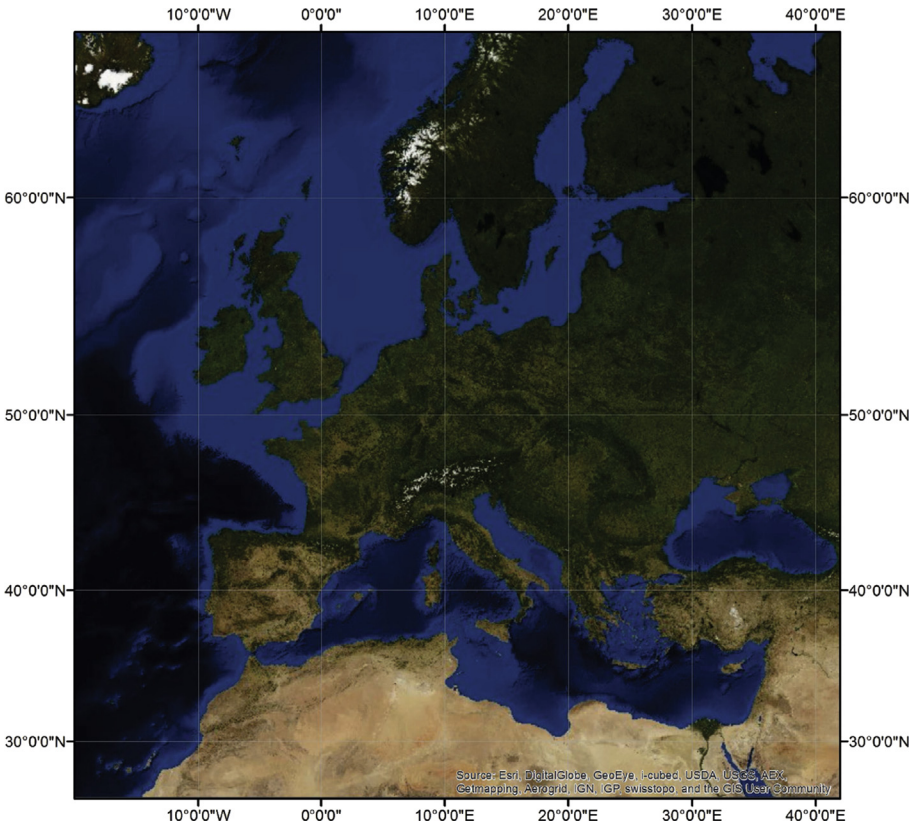

Fig. 2. The SKIRON and WAM model domain.

over which a maximum value is identified and λ is the rate of occurrence, calculated with

$$\lambda = \int_0^\infty P(x,\dot{x})\dot{x}d\dot{x} = \frac{\sigma_{\dot{x}}}{\sqrt{2\pi}}P(x), \tag{1}$$

with $P(x,\dot{x})$ the conditional probability of x, $P(x)$ the probability of x, $\dot{x}$ the time derivatives of x, and it is assumed that x and $\dot{x}$ are independent. With a large threshold, such a distribution of the exceedance is valid for a Gaussian process for which

$$P(x) = \frac{1}{\sigma_x\sqrt{2\pi}}\exp\left(-\frac{x^2}{2\sigma_x^2}\right). \tag{2}$$

Substituting Eq. (2) to Eq. (1) gives

$$\lambda = \frac{1}{2\pi}\frac{\sigma_{\dot{x}}}{\sigma_x}\exp\left(-\frac{x^2}{2\sigma_x^2}\right). \tag{3}$$

Equation (3) can be re-written as

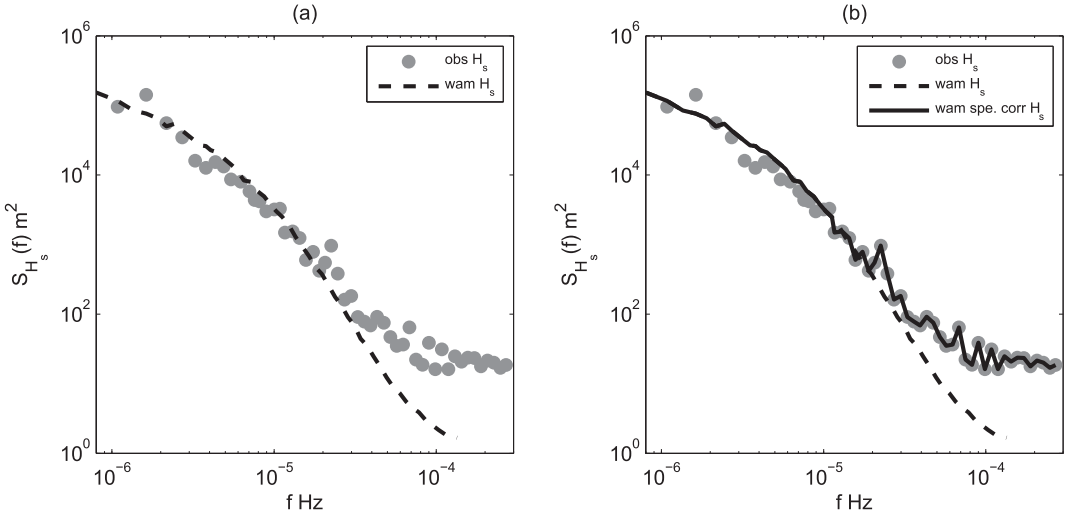

Fig. 3. (a) Power spectra of measured and modeled significant wave height at FINO 1. (b) Combination of the observed and modeled spectra to obtain the full spectrum (solid black curve), on top of (a).

$$\lambda = \frac{1}{2\pi}\sqrt{\frac{\overline{m_2}}{m_0}}\exp\left(-\frac{x^2}{2m_0}\right), \tag{4}$$

with the spectral moments, m_0 and m_2, defined as

$$m_j = 2\int_0^\infty \omega^j S(\omega)d\omega, \tag{5}$$

Here $S(\omega)$ is the power spectrum of the Gaussian process x and $\omega = 2\pi f$, with f the frequency in Hz. Note that $x = x_{ts} - \overline{x_{ts}}$, with $\overline{x_{ts}}$ the mean value of the original time series of variable x_{ts}.

For the maximum value that occurs once a year, $\lambda T_0 = 1$. Together with Eq. (4), it gives

$$X = \overline{x_{ts}} + \sqrt{m_0}\sqrt{2\ln\left(\frac{1}{2\pi}\sqrt{\frac{\overline{m_2}}{m_0}}T_0\right)} \tag{6}$$

The variation in the high frequency range does not affect $\overline{x_{ts}}$, brings small difference to the standard deviation ($\sqrt{m_0}$), but contributes significantly to m_2 and, therefore, to the maximum value X as shown in Eq. (6).

The core of the spectral correction approach is to replace the tapered-out spectrum (e.g. the dashed line in Fig. 3a) with the measured one (the dot-curve in Fig. 3a), if measurements are available. The frequency range to be corrected starts at the point where the modeled spectrum deviates from the measured one and ends at the required resolution. If the targeted temporal resolution is one hour as the modeled data, then the correction should be done to $2\cdot10^{-5} < f < 11.2\cdot10^{-4}$ Hz. Here the measurements are half hourly, so that the Nyquist frequency is $5.6\cdot10^{-4}$ Hz. In this study the correction is thus done to this range $2\cdot10^{-5} < f < 5.6\cdot10^{-4}$ Hz. If measurements are not available, a spectral model is needed to be developed for the wave conditions at a particular location. Thus, with a spectrum of non-corrected high frequency range (the dashed curve in Fig. 3a and b), one obtains the first set of m_0 and m_2; together with the corresponding mean value $\overline{x_{ts}}$, Eq. (6) gives the maximum value of X_1. Now, with the corrected spectrum (the thick, solid curve in Fig. 3b), one obtains a new set of m_0 and m_2. Together with the corresponding mean value $\overline{x_{ts}}$, Eq. (6) gives another maximum value, X_2.

Based on the relation of H_s^{max} and the T-year return value, H_s^T, (see the next section Eq. (11)), the relative underestimation in the dataset of H_s^{max} should in principle be the same as that of H_s^T for $T \gg 1$ year. The underestimation due to "smoothing effect" is defined as:

$$SE = 1 - X_1/X_2. \tag{7}$$

5. The statistical methods for extreme wave height

In the estimation of the 50-year return value, the generalized extreme value distribution (GEVD) and the generalized Pareto distribution (GPD) are two popular functions.

The GEVD for fitting the extreme values in the form of maximum from a basis period T_{BP} takes the form:

$$F(X) = \exp\left(-(1-\alpha k(X-\beta))^{1/k}\right), \tag{8}$$

where $F(X)$ is the probability that X is not exceeded during the basis period, k is a shape factor, α and β are distribution parameters. The distribution is known as Type III (or reverse Weibull) extreme value distribution when $k > 0$, Type II (or Frechet) extreme value distribution when $k < 0$ and Type I (or Gumbel) distribution. Only Type III provides limiting return value at high T and Type II quickly leads to a very high estimation.

The GPD is used to describe the exceedances over a threshold x_0 and it takes the form:

$$F(X, x_0) = 1 - \left(1 - \frac{k(X-x_0)}{A}\right)^{1/k}, \tag{9}$$

where A is a scale factor and k is the shape factor.

The determination of the shape factor k is rather empirical and it is highly sensitive to the selected samples. The uncertainty becomes particularly high when the samples are possibly contaminated by e.g. the dependence on each other or/and the different mechanisms [30]. For the above reasons, we choose Type I distribution of both GEVD and GPD to estimate the 50-year return value of the significant wave height, H_s^{50}. Thus, related to GEVD we use the Gumbel distribution for the maximum values from a basis period, denoted as the Periodic Maximum Method (PMM) [18]. Related to GPD, we assume a Poisson process to describe the independent peaks over a threshold, denoted as the Peak-over-Threshold (POT) method. The two methods are described in sections 5.1 and 5.2, respectively. Whether it is a reasonable assumption to use $k = 0$ is validated here through the "goodness-of-fit" analysis. The procedure of the "goodness-of-fit" analysis is from the so-called Kolgomorov–Smirnov test. If the largest difference between the observed and predicted distribution function, $\Delta F(X)$, is less than a critical value, e.g. here we use $1.36/\sqrt{n}$ (related to the 95% confidence interval, where n is the sample size), then the fitting passes the "goodness-of-fit" test [2,30].

Both PMM and POT methods are being used in the wave data analysis [10,50]. It was demonstrated that the two methods give consistent results when used appropriately [30]. Compared to POT for which the choice of the threshold and the definition of independent samples are important but not straightforward, PMM is a much simpler approach [30]. Here, due to the limited data length (especially Horns Rev) and data coverage (especially FINO 1), using two different methods instead of one gives a broader overview of the uncertainties in the estimation of H_s^{50}.

5.1. The periodic maximum method (PMM)

In this method, the Gumbel distribution is used to fit the extreme wave height samples from a basis period T_{BP}, $H_{s,i}^{max}$, where $i = 1, \ldots, n$, with n the number of samples:

$$F(X) = \exp(-\exp(-\alpha(X-\beta))) \tag{10}$$

Relating $1/(T\cdot T_{BP}^{-1})$ to $1 - F(X)$ gives the T-year return value for the Gumbel distribution at relatively large T as:

$$H_s^T = \alpha^{-1}\ln\left(T\cdot T_{BP}^{-1}\right) + \beta \tag{11}$$

where α and β are obtained with the probability-weighted moment procedure [2,20]:

$$\alpha = \frac{\ln 2}{2b_1 - \overline{H_s^{max}}}, \quad \beta = \overline{H_s^{max}} - \frac{\gamma_E}{\alpha} \tag{12}$$

where $\gamma_E \approx 0.577216$ is Euler's constant, and $\overline{H_s^{max}}$ is the mean of $H_{s,i}^{max}$. b_1 is calculated from

$$b_1 = \frac{1}{n}\sum_{i=1}^{n}\frac{i-1}{n-1}H_{s,i}^{max} \tag{13}$$

The variance of X can be described as $Var(X) = \pi^2/(\alpha^2 6)$. The natural range of magnitude of X depends on the variable; the reported, observed highest waves in the world are 20–30 m.

According to [2] and [20]; this probability-weighted moment procedure gives less bias and variance on the estimates, compared to the least square regression method. It has been proven to be highly efficient even for small size samples. However, here the calculation is not very different from using the least squares linear regression.

Note that the choice of T_{BP} should ensure the selected extreme events are from the same mechanism. In our case, we have used T_{BP} as half year for Horns Rev where the measurements have good coverage but the record is short, and we have used T_{BP} as one year for FINO 1 where the data coverage is relatively poor but the record is long. One may argue if using 6 months introduces the seasonal bias to the samples. This should not be a problem for Horns Rev here because the maximum values, identified from the first and second half year, are from winter storms only. Once it is ensured that no two samples from the same storm, it is a reasonable solution to make best use of the relatively short time series.

The standard error of the fitting in obtain H_s^T can be calculated from the standard deviation of H_s^{max} [2,36]:

$$\sigma\left(H_s^T\right) = \frac{\pi}{\alpha}\sqrt{\frac{1 + 1.14k_T + 1.10k_T^2}{6n}} \tag{14}$$

where

$$k_T = -\frac{\sqrt{6}}{\pi}\left(\ln\ln\left(\frac{T}{T-1}\right) + \gamma_E\right). \tag{15}$$

[28] showed that the T-year estimate can be assumed to be normally distributed. Accordingly, the 95% confidence interval can be estimated to be $1.96 \cdot \sigma(H_s^T)$.

5.2. The peak-over-threshold method (POT)

When using the POT method, the peaks over a threshold x_0 should be independent of each other. This can be ensured by requiring two consecutive peak values be separated from each other with an interval. The peak values of H_s here are related to the mid-latitude cyclones. Based on observations, a mid-latitude cyclone is of the duration of several days. Thus, setting the interval as 7 days could be considered as an appropriate start. A range of the intervals from 7 days to 14 days were tested and the final estimate did not show to be sensitive to the values in this range. The results presented here are based on such an interval of 10 days; namely, the identified two consecutive peaks are at least 10 days apart. Some studies have assumed the storms to be separated from each other by 2 days, e.g. Ref. [11]. In Ref. [16]; the autocorrelation of the time series was calculated when looking for such an interval to ensure samples are independent of each other. The similar calculation has been done using H_s from months when the data coverage is 100%. The autocorrelation of H_s becomes less than 0.5 at two days and turns to be about zero at four days, suggesting that our choice of the interval as 10 days is sufficiently long to ensure the consecutive cases being independent. These samples that satisfy the Poisson process are described by the Type I distribution:

$$F(X) = 1 - \exp\left(-\frac{X - x_0}{A}\right) \tag{16}$$

If the exceedance rate of the level x_0 is λ per year, then the mean crossing rate of the level H_s^T is $\lambda(1-F)$. The variance of X is A^2. Relating $1/T$ to $\lambda(1-F)$ gives

$$H_s^T = x_0 + A\ln(\lambda T) \tag{17}$$

For a Poisson process and properties of the exponential distribution, the uncertainty of the fitting can be estimated from the propagation of variance formula [2,36]:

$$\sigma\left(H_s^T\right) \approx \frac{A}{\sqrt{\lambda L}}\sqrt{1 + \ln^2(\lambda T)} \tag{18}$$

where L is the data length in year.

With the same argument of the distribution of the T-year estimates as for PMM, the 95% confidence interval is $1.96 \cdot \sigma(H_s^T)$.

6. Data validation and results

In section 6.1, first, the standard statistics of the distribution of modeled H_s (denoted as $H_{s,m}$) are studied in terms of scatter plot for both sites. It will be shown that the modeled H_s is satisfactory for the relatively deep water, open water site FINO 1 but is overestimated for the shallow water, coastal site Horns Rev. To find out where the deviation occurs, for Horns Rev, further examinations were done to the probability density function (PDF) of the time series. In addition, the time varying parameters, consisting of wind speed and direction, wave direction and H_s, were examined through a number of storms, which we took as the 5 strongest as examples from each year from 2001 to 2006 from available measurements. To demonstrate the issue of the smoothing effect on the time series of H_s, as discussed section 4, H_s is afterwards examined in the spectral domain.

The analysis in section 6.1 leads to the conclusion that a post-processing procedure is necessary to handle the modeled H_s before using it to estimate H_s. This post-processing procedure is explained in section 6.2 and the results of H_s^{50} are shown in section 6.3.

6.1. Wave height statistics

The scatter plot of the observed and modeled significant wave height, $H_{s,o}$ and $H_{s,m}$, respectively, were plotted for FINO 1 and Horns Rev in Figs. 4 and 5. In Fig. 4, a linear regression is made and it overlaps with the curve showing 1:1, suggesting a good agreement with the observed and modeled data at FINO 1. On the other side, Horns Rev site (Fig. 5a) gives an immediate message that a reasonably good agreement with little bias only exists for a very narrow range of H_s where $H_s < 1$ m, and at higher values, $H_{s,m}$ is obviously overestimated.

This clearly shows the difference in the model's ability for open water, relatively deep waters and coastal, shallow waters. In connection with the two statistical methods for estimate of H_s^{50}, PMM and POT, it is highly relevant to find out the quality of the wave simulations during individual storms at Horns Rev. The storms that are used for examining this quality were identified from the available wind measurements at 62 m from a meteorological mast [32]. The five strongest storms from each year from 2001 to 2006 were selected. For each of the storms, the time series of the wind speed (at 15 m from measurement, at 10 m as derived using the second order polynomial fit to measured wind speeds at 15, 30, 45 and 62 m and at 10 m for SKIRON data), wind direction, wave direction and H_s are examined. The strongest storm from each year is plotted in Fig. 6 as an example. The analysis of the time series during the 30 storms shows that: (1) For the wind speed, the agreement between model and measurements is rather good, considering the strength and phase. Occasionally the measured and modeled winds can be out of phase for several hours (e.g. 2001–02–03 to 2001–02–07, not shown). (2) The modeled and measured wind direction is in rather good agreement, but deficiency can also occur (e.g. Fig. 6f). The wave direction is often along the wind direction but it can deviate quite significantly from the

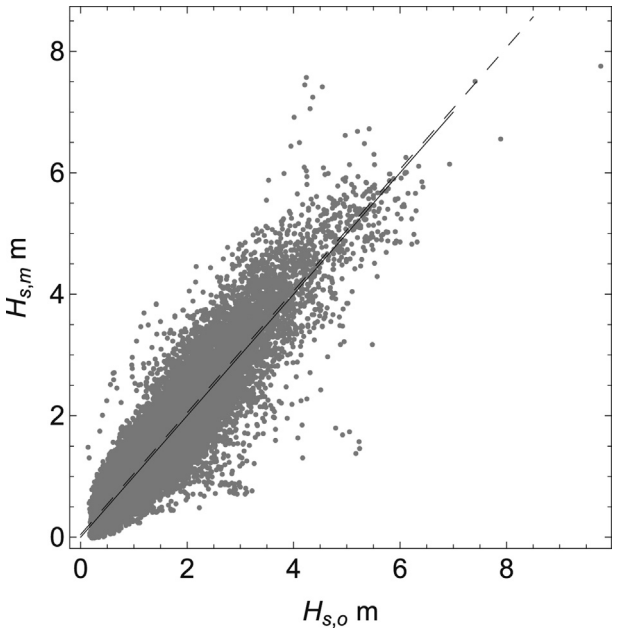

Fig. 4. Scatter plot of observed and modeled significant wave height, $H_{s,o}$ and $H_{s,m}$, respectively at FINO 1. The dashed line shows the linear regression. The solid lines show 1:1.

wind when the winds change direction suddenly (see Fig. 6d and f for an example). When wind direction suddenly changes, the swell component of the waves is still influencing the mean wave direction. (3) Accompanying the peaking of the wind speed, H_s also forms a peak. However, the model significantly overestimates H_s for all storm peaks at Horns Rev.

The overestimation of the WAM simulated H_s is also seen in the PDF (Fig. 7). The modeled and measured data in their overlapping period from each year were used to calculate the PDF. For all six years, the tails of $H_{s,m}$ suggest a large number of high values (thin, dashed curves) that are absent in the PDF of $H_{s,o}$ (gray curves).

The time series of $H_{s,m}$ was accordingly studied in the spectral domain, together with the measurements $H_{s,o}$.

For FINO 1, the mean statistics of $H_{s,m}$ has shown to be in good agreement with that of $H_{s,o}$ (Fig. 4), and the power spectrum of $H_{s,m}$ is in good agreement as well with that of $H_{s,o}$ for frequency f less than about $2 \cdot 10^{-5}$ Hz, see Fig. 3a. However, the power spectrum tappers out for higher frequencies, as discussed in section 4.

For Horn Rev, the tapered-out spectrum is present, too, as can be seen in Fig. 8. In addition, corresponding to the overestimated H_s for relatively high waves, the low frequency power spectrum of $H_{s,m}$ is overestimated too. The increased variance in the low frequency range leads to elevated standard deviation and, eventually contributes to the overestimation of the extreme value, together with the overestimated mean values.

For FINO 1, the spectrum of H_s was calculated with data with each month where data coverage is 100% (Table 3) and averaged afterwards (dots in Fig. 3). For Horns Rev, the spectrum was calculated with each month where data coverage is 99.9% and averaged afterwards (dots in Fig. 8).

The following section discusses solutions to applying $H_{s,m}$ for further applications.

6.2. The post-processing procedure

The post-processing procedure aims at achieving expected mean as well as spectral statistics for the modeled data in both the low and high frequency ranges.

The comparison of Figs. 3 and 8 shows the issues at the coastal shallow water site Horns Rev at lower frequencies. Clearly, for Horns Rev, both the low and high frequencies need to be taken care of in order to obtain a reasonable estimate of the extreme value.

For FINO 1, the low frequency spectrum does not need to be corrected (Fig. 3a) and the correction is applied to the high frequency part only (Fig. 3b). For Horns Rev, the low frequency part can be corrected through a linear regression of the modeled time series to the measured, the result is the matching statistics for the mean and standard deviation (Fig. 8a, the dashing curve). Afterwards, we make the spectral correction for the high frequency part (Fig. 8b, the solid curve).

The following demonstrates how a linear regression corrects the mean statistics and accordingly the low frequency spectrum, for Horns Rev.

Figs. 5a and 7 show that $H_{s,m}$ and $H_{s,o}$ differ mostly for $H_s > 1$ m. For $H_s < 1$ m, due to the good agreement between $H_{s,m}$ and $H_{s,o}$, the H_m values will be kept unchanged. For $H_s > 1$ m, by requiring the regression line crossing the coordinate (1, 1) in order to make

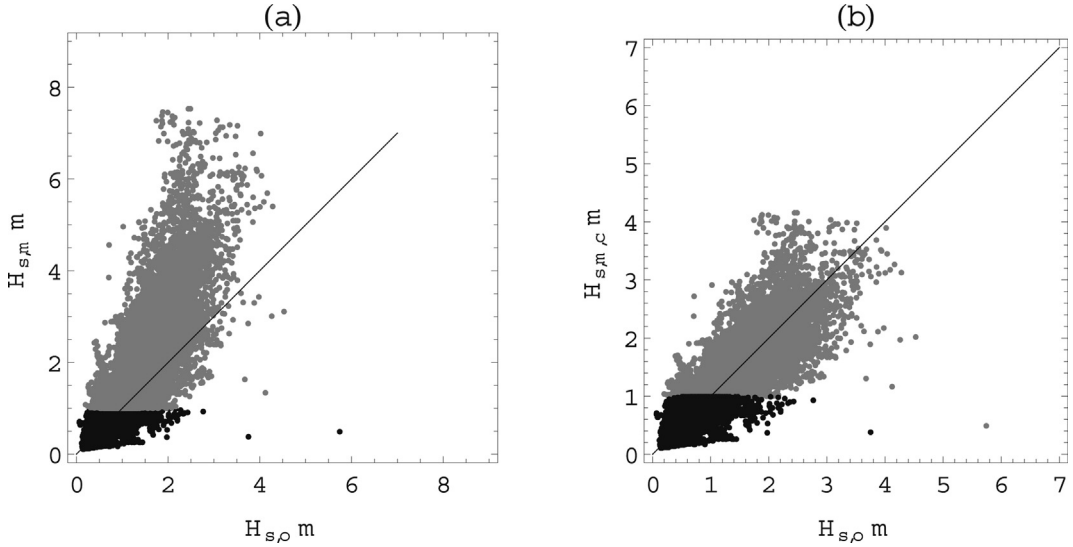

Fig. 5. Scatter plot of observed and modeled significant wave height, $H_{s,o}$ and $H_{s,m}$, respectively, at Horns Rev. (a) with H_s from WAM directly. (b) with H_s corrected using Eq. (19). The data are divided into two groups according to H_s : $H_s \leq 1$ m (black) and $H_s > 1$ m (gray). The lines show 1:1.

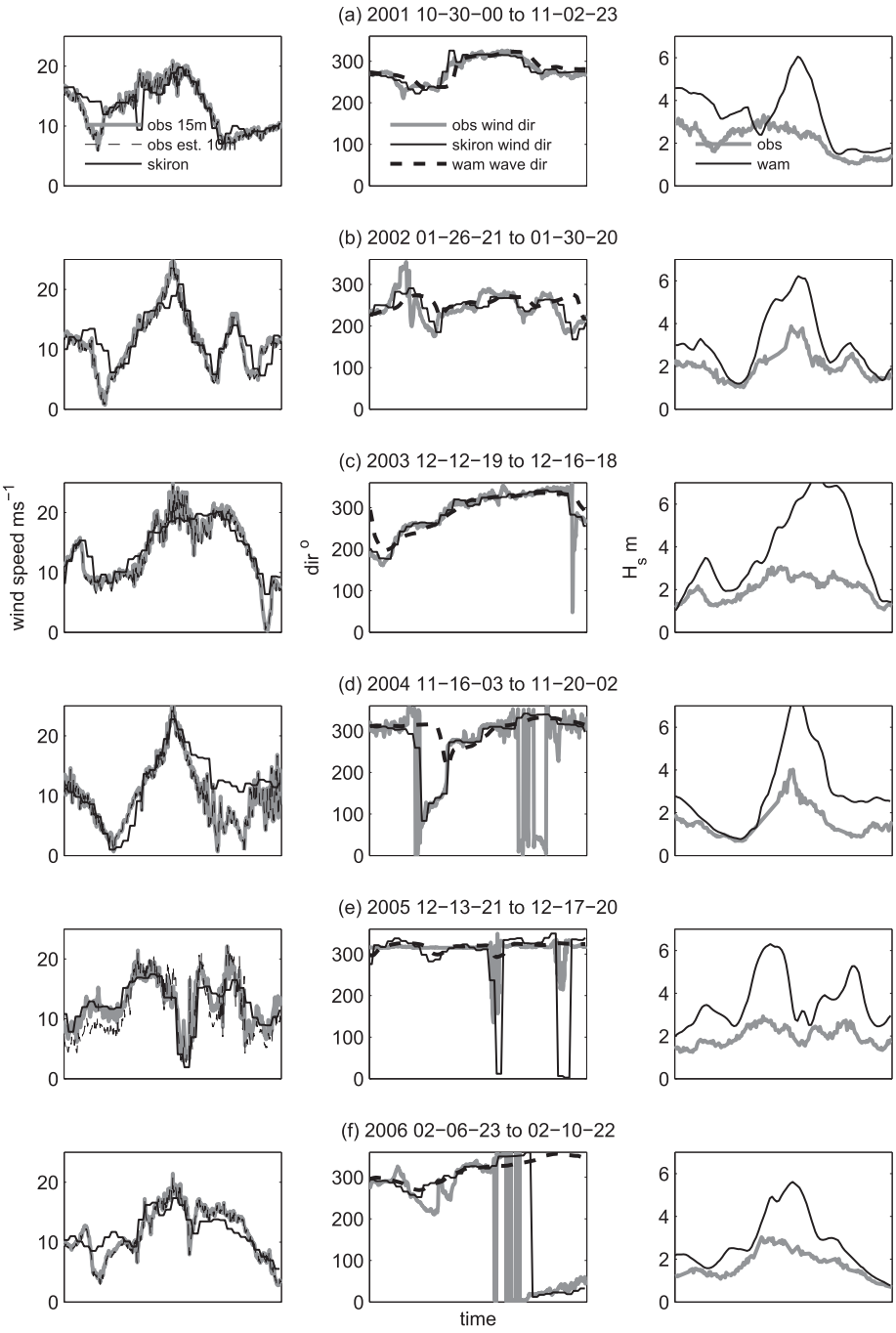

Fig. 6. Data from the Horns Rev site. left column: time series of wind speed; middle column: mean wind direction and mean wave direction, and right column: significant wave height H_s, for the strongest storm from the year 2001–2006 where measurements are available.

continuous transition to the range of $H_s < 1$ m, a least square linear regression has been done to the scatter plot of $H_{s,m}$ versus $H_{s,o}$, and a set of coefficients, a_1 and b_1, are obtained: $H_{s,m} = a_1 H_{s,o} + b_1$. To reduce the bias caused by the regression fitting, similar regression has been done to the scatter plot $H_{s,o}$ versus $H_{s,m}$ and another set of coefficients is obtained: $H_{s,o} = a_2 H_{s,m} + b_2$. Averaging the two, with the condition that the line passing the coordinate (1, 1), we obtain the following relationship between $H_{s,m}$ and $H_{s,o}$:

$$H_{s,o} = \frac{H_{s,m} - (1-a)}{a}, \tag{19}$$

and a =2.07 was obtained for this data set. Thus, a corrected time series, $H_{s,m,c}$, can be obtained from $H_{s,m}$ and a through Eq. (19) where $H_{s,m,c} \approx H_{s,o}$. The mean value of the modeled time series is thus corrected to the level of measurements. The corrected significant wave height $H_{s,m,c}$ is now plotted versus $H_{s,o}$ in Fig. 5b, also in gray, and the bias is seen to be greatly reduced. In doing so we manually put weight on the group of large values. As an exercise, a single regression using a second-order polynomial has been done to the entire dataset. Whereas the results are similar, it is foreseen that such a single regression can sometimes miss the largest values because it is weighted mostly to the data range of highest density, which are not necessarily the largest values.

As a result, the PDF of $H_{s,m,c}$ now matches much better with $H_{s,o}$, shown in Fig. 7 as the thick black curves, including the skewness

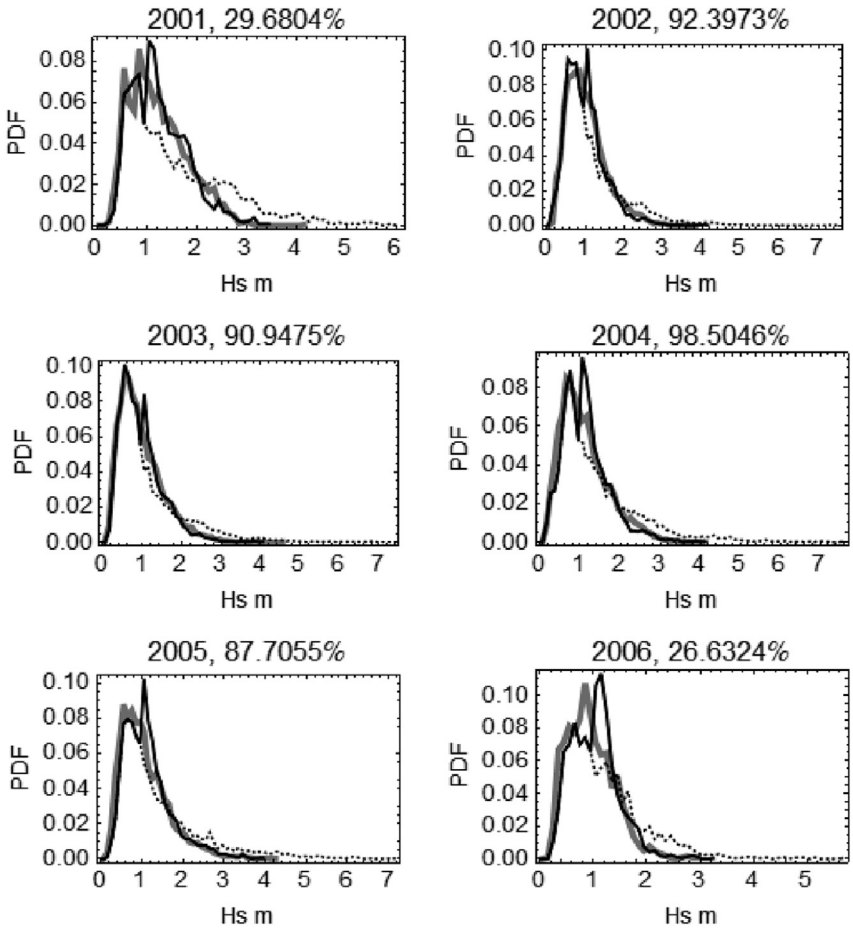

Fig. 7. PDF of the significant wave height H_s for the overlapped data from measurements (gray curves) and WAM (black dashed curves) for the Horns Rev site, for each year. The solid, black curves are from the corrected time series using Eq. (19). The data coverage from each year is given in the subplot title. The H_s-bin width is 0.1 m.

and tail behavior. At the same time, the overestimated energy level in the power spectrum (the solid, black curve in Fig. 8b) for $f < 2 \cdot 10^{-5}$ Hz has also been corrected and it now matches well that of the measurements (the dashed, thick black curve). This ensures that m_0 is corrected for the low frequency range. Linear regression has earlier been used in Ref. [12] to "correct" the modeled data and has been used in and [47] to correct the return value estimates. The regression will not help resolving the high frequency variability, as expected.

The "smoothing effect" in the high frequency range *SE* was estimated by the spectral correction method as described in section 4 to be 6% at FINO 1 and 7% at Horns Rev.

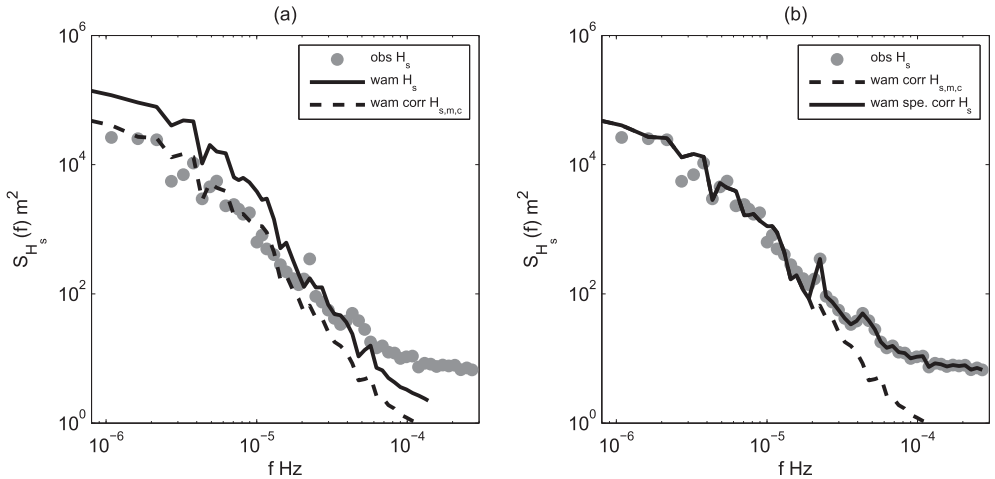

Fig. 8. (a) Power spectra of observed and modeled significant wave height at Horns Rev, and regression-corrected significant wave height from model. (b) Combination of the measured and modeled spectra to obtain the full spectrum (solid black curve).

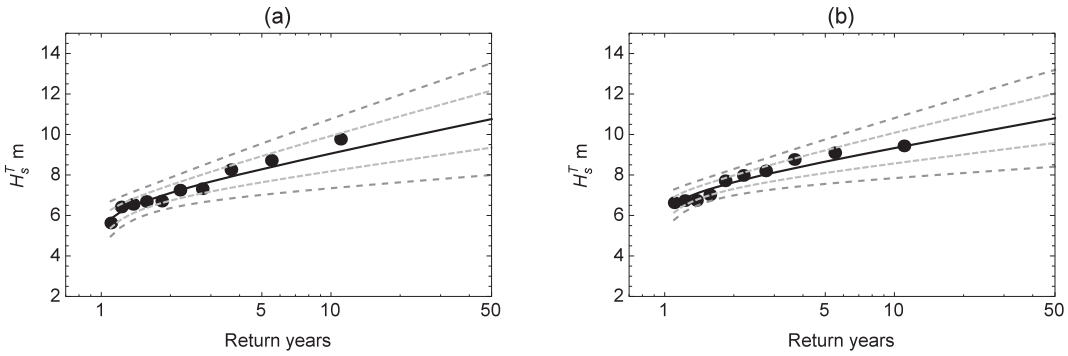

Fig. 9. T-year return value of H_s at FINO 1, using PMM. (a) with H_s from measurements. (b) with H_s from WAM for 2001 to 2010, with the spectral correction.

6.3. Extreme wave height

The 50-year significant wave height, H_s^{50}, has been calculated using the PMM and POT methods for the two sites FINO 1 and Horns Rev. The results are presented in section 6.3.1 and 6.3.2, respectively.

6.3.1. FINO 1

The measurements at FINO 1 are long but the data coverage during some years is rather poor. The basis period was chosen to be 1 year when applying PMM. We used data from 2004 to 2013. Fig. 9a shows the distribution of the annual maximum $H_{s,o}$, together with the Gumbel distribution and the uncertainties (the dashing curves on the outside showing the 95% confidence intervals, $H_s^T \pm 1.96 \cdot \sigma(H_s^T)$, and those inside are $H_s^T \pm \sigma(H_s^T)$). Fig. 9b shows the corresponding information for the annual maxima $H_{s,m}$, where the spectral correction was applied, adding 6% to H_s^{50}.

Fig. 10a and b shows the data distribution using POT method. The threshold selection is of major importance. A high threshold can result in a small amount of exceedances for the application. Concerning that the flexibility and possibility of collecting relatively large sample is the advantage of using POT method compared to PMM, the threshold should not be too high. A low threshold, on the contrary, will lead to larger amount of exceedances, which, at the same time, has a possibility to introduce "penetration" of a second population of extremes to the sample. This second population carries different characteristics and may affect the overall distribution of samples. According to Eq. (18), the selection of the threshold, together with the separation time that is used between events, will affect the calculation of the scale factor and crossing rate and therefore the fitting uncertainty. A proper selection of the threshold can be done through the help of certain tools such as the quantile plots or goodness-of-fit tests such as the Kolgomorov–Smirnov or Darling-Anderson test. For FINO 1, the threshold was taken as the 99% percentile of H_s and we used the "goodness-of-fit" as introduced in the end of section 5 to ensure the best fit.

Table 4 lists H_s^{50} calculated from the PMM and POT methods, each in 4 groups. Group-a is the calculation using measurements 2004 – 2013. Group-b is from the entire modeled time series with spectral correction. Group-c is from the modeled data of the overlapping period with measurements. Group-d is from the entire modeled time series without spectral correction. The values from group-d are smaller than group-b, reflecting the smoothing effect of the modeling.

With the smoothing effect corrected, the estimates of H_s^{50} using PMM are consistent with those using POT. The agreement in H_s^{50} between the measured data and the modeled data (with spectral correction) can be considered good for this relatively deep, open water site, even though uncertainties are present due to limited measurement coverage.

The overall magnitude of H_s^{50} is on the order of 10.8 m. Comparing to the atlas of the 50-year return significant wave height based on the Altimeter data over the North Sea (Fig. 2 in Ref. [51]); this is an excellent agreement. Note that the Altimeter data correspond to a coarse horizontal resolution of about 2°.

6.3.2. Horns Rev

Similar calculations as for FINO 1 have been done to Horns Rev, except that the basis period is chosen to be 6 months when using PMM, with one sample from the first half year and one sample from the second half year. This adjustment is made because the data length is short but the coverage is good. Using 6 months as the basis period is not suitable for FINO 1 because the poor data coverage indicates a higher chance to miss the peak value from a shorter basis period. The distribution of the half-year maxima is shown in Figs. 11 and 12, for measured and modeled values, respectively. Compared to Figs. 9 and 10, we added the plots of the modeled data from the overlapping period (plots-c) to see how much the short

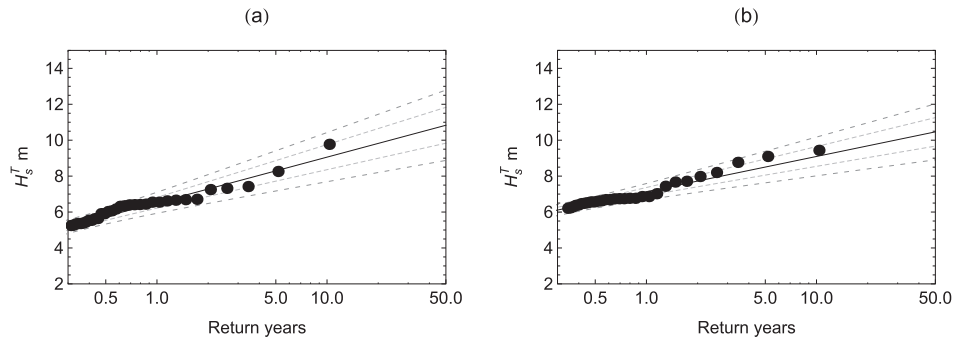

Fig. 10. At FINO 1. The same notation as Fig. 9, except that the results are from the POT method.

Table 4
H_s^{50} at FINO 1, together with $\sigma(H_s^T)$ from PMM and POT for four groups of data: group-a is for measurements; group-b is for the modeled H_s with post-processing for the entire 10-year simulation; group-c is for the modeled H_s with post-processing for the overlapped time with measurements in a; group-d is for the modeled H_s without post-processing for the entire simulation period.

	$H_s^{50}\pm\sigma$ (m)	
	PMM	POT
a	10.8±1.0	10.8±2.0
b	10.8±1.1	10.5±1.6
c	11.2±1.1	10.5±1.9
d	10.2±1.2	9.6±1.5

data length affects the data distribution. We also added the plots calculated directly from the modeled data without the spectral correction, in order to get an insight of the overestimation of H_s at this shallow water site.

The estimates of H_s^{50} are listed in Table 5 in the same manner as Table 4.

Measurements (group-a) and the post-processed model data (group-b) give rather similar results of H_s^{50}; group-c, the modeled data from the overlapping period, gives slightly smaller values. Note that 5-year is rather a short period for an estimate of 50-year return value, as will be discussed in Section 6. Nevertheless, this gives an idea how the measured and modeled data agree with each other on this subject. The difference in H_s^{50} between group-c and group-b is significantly smaller than the 95% confidence intervals. Without the post-processing, the modeled data significantly overestimates H_s^{50} (group-d).

It should be pointed out that when using the POT method, the 98%-percentile value of H_s was used as the first attempt as the choice of the threshold x_0. The reason of choosing 98% instead of 99% percentile as for the FINO 1 data is to collect sufficient samples, since the time series is a lot shorter for the Horns Rev data. Values around the first attempt were tested in order to obtain the smallest value of $\Delta F(X)$. Accordingly, group-a, b and c passed the goodness-of-fit where $x_0 = 2.1$ m, 3.0 m and 3.0 m were used, respectively. For group-d, the 98%-percentile did not give a goodness-of-fit, so a number of values around it were tested and eventually $x_0 = 5$ m gave a set of samples that passed the goodness-of-fit test.

The overall magnitude of H_s^{50} is on the order of 6 m. Comparing to the atlas of H_s^{50} based on the Altimeter data (Fig. 2 in Refs. [51]); this is also an excellent agreement.

7. Discussion

Within the framework of the EU MARINA Platform project, one of the objectives is to estimate the extreme waves using output from high resolution wave-atmosphere coupled model, with shallow water effect considered.

It is obvious that existing modeling systems need further improvement in dealing with the coastal issues. However, any numerical wind or wave model will never be perfect in describing very local phenomena due to parametrization reasons and the inability to simulate successfully subgrid scale processes. At the same time, the current study does not focus on the wave model development but on their application/exploitation for local activities.

Existing atlases are of horizontal resolutions from 10 km to more than a hundred of kilometers. The wave model WAM used here was run at a horizontal resolution of 5 km, for 10 years period. For such a large domain (Fig. 1), this is an extensive setup. In the present work, the ECMWF parallel version, CY33R1 [22] of WAM has been used. A number of new features are included in this version that makes it possible to simulate the wave propagation even at shallow water sites. This latest version of WAM has been reported to perform comparably well with the coastal model SWAN at high resolution [9,48]. Numerous work has reported good performance of WAM for deep water conditions, when standard mean statistics were examined. The calculation of the extreme H_s atlas extended to the coastal areas [1,10] but there lack evidences of their reliability.

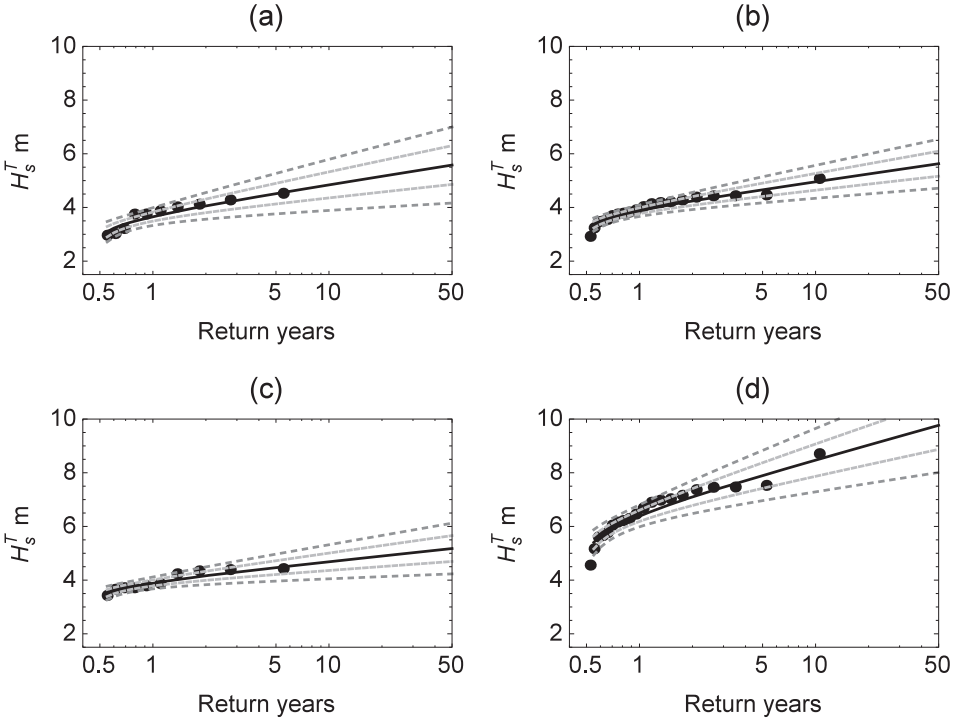

Fig. 11. T-year return value of H_s at Horns Rev, using PMM. (a) with H_s from measurements. (b) with H_s from WAM for 2001 to 2010, post-processed. (c) with H_s from WAM overlapping with measurements, post-processed. (d) with H_s from WAM, no post-processing. In each plot, the dashed curves are $H_s^T \pm 1.96 \cdot \sigma(H_s^T)$ (outside) and $H_s^T \pm \sigma(H_s^T)$ (inside).

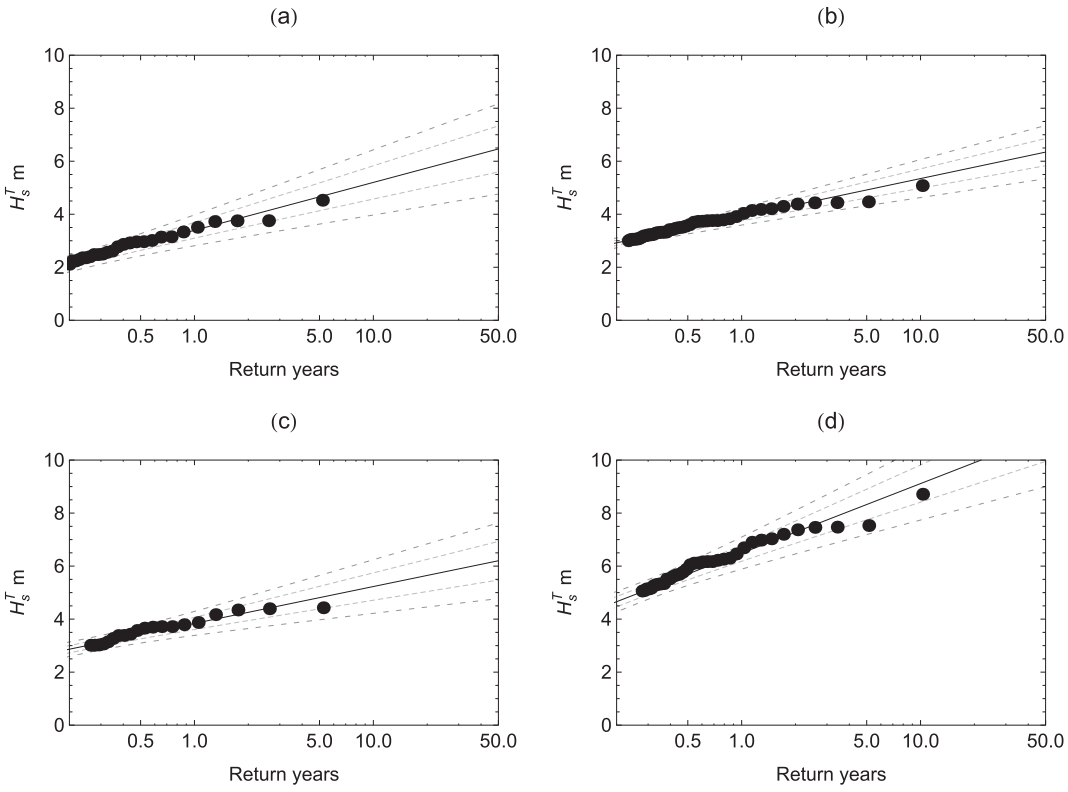

Fig. 12. At Horns Rev. The notations are the same as Fig. 11, except that the results are from the method of POT.

The data analysis in this study, performed at an open and relatively deep water (FINO 1) as well as a coastal, shallow water site (Horns Rev), demonstrates clearly that WAM is capable of reproducing the wave climate at FINO 1 but is challenged by the complex coastal shallow water, like Horns Rev. This is reflected as the overestimation of mean H_s during storm conditions, a phenomenon being frequently documented, e.g. Refs. [14,25,39]. The issue of the swell decay can be considered as a key contributor to this, which is especially problematic in the coastal shallow waters [49]. The challenges in the coastal area are not only present for WAM but also for the coastal models such as SWAN and MIKE 21 SW [48]. Possibly, an even finer model resolution is likely required here for further investigation. In connection with the analysis of extreme wave parameters under North Atlantic extratropical cyclones, [33] discussed several possible mechanisms that are responsible for the formation of the extreme waves. They also discussed the literatures regarding the model setups in taking these mechanisms into account in order to improve the numerical prediction of storms and hence extreme wave heights. It is important to note at this point that some classical hypotheses made in numerical modeling, with the purpose to obtain probability distributions that optimally describe wave heights, may also contribute to direct model output discrepancies, see e.g. Refs. [38,45] and [33].

Table 5
H_s^{50} at Horns Rev, together with $\sigma(H_s^T)$ from PMM and POT for four groups of data: group-a is for measurements; group-b is for the modeled H_s with post-processing for the entire simulation period; group-c is for the modeled H_s with post-processing for the overlapped time with measurements in a; group-d is for the modeled H_s without post-processing for the entire 10-year simulation.

	$H_s^{50}\pm\sigma$ (m)	
	PMM	POT
a	5.6±1.4	6.5±1.7
b	5.6±1.0	6.3±1.0
c	5.2±1.0	6.2±1.4
d	9.8±1.8	10.9±2.0

It was demonstrated here that through simple linear regression, with only limited measurements, we can correct the modeled H_s in the complicated shallow water site to obtain matching spectral statistics, including both the low and high frequencies. The novelty of this study is to, for the first time, apply the spectral correction method to the time series of H_s, in order to feed in the missing variability in the high frequencies. A number of months with full data coverage is sufficient in providing a spectrum for such a correction. Unless a model is run at such a high resolution that it physically resolves the small-scale wave activities that are related to, possibly, the local wind–wave interaction bounded by the wind and wave directions, the topography, the bathymetry and non-local long waves, such a spectral correction is needed. The smoothing effect from the 5 km resolution model output for the two sites examined here is about 7% when corrected to half hour resolution; it is expected to be greater if the model resolution is coarser.

It is still too early to conclude whether the final estimates of H_s^{50} here are sufficiently accurate for the two sites, because there lack long term measurements for data validation. It is not an easy task to have access to long term wave measurements with consistent quality. The use of sufficiently long term data is not only for collecting many enough samples for making a good fit for Eq. (11) and Eq. (17), it is also needed to take into account of the climatological variability of the variable [30]; here H_s. Plotting the annual maximum $H_{s,o}$ and $H_{s,m}$ from FINO 1 shows two peaks in 10 years in both (not shown), indicating a possible long term period on the order of 5 years and a time series of shorter than 5 years would imply significant bias. However, the climatological representativity of 5 years, or 10 years, of data can only be accessed through a much longer measurement record, say 30 years.

On the other hand, the excellent agreement with the results from the 11-year Altimeter data [51] for the two sites indicates that our estimation is in the right direction but the Altimeter data is of rather coarse resolution and its uncertain in the coastal area requires further investigation.

8. Conclusions

This study aims to provide a validation and optimization procedure for wave modeling data related to extreme value estimation suitable for applications in offshore renewable energy issues. The methodology proposed examines not only the mean values of the wave parameters, such as significant wave height, but also their spectral properties. In particular:

- The smoothing effect of modeling is present both for deep water and shallow water conditions and it needs to be corrected.
- WAM performs excellently for the intermediate to deep water site FINO 1.
- WAM over-predicts mean H_s during storms for the coastal, shallow water site, which affects the calculation of the extreme wave height. This overestimation can be easily corrected with limited measurements through linear regression.
- For the analysis of the local wave extreme conditions, especially for near-shore areas, the information provided by numerical wave models, even on high resolution versions enabled with shallow water features, is not always enough, since complicated dynamical wind–wave interaction processes are not satisfactorily simulated, particularly during storm events. The use of statistical post-process for local adaptation significantly optimized the model outputs. In particular, the spectral correction method, utilizing up to the second order moment of the spectrum, leads to improved results compared to simple linear regression models.
- The 50-year significant wave height was estimated as a characteristic measure for the extreme value events, through the use of long term modeled data that are post-processed with the help of limited measurements. The final results show good agreement with the 50-year return values estimated from the Altimeter data from earlier studies.

Acknowledgment

This study is supported partly by the EU Marina Platform project and partly by the Danish project X-WiWa (PSO-12020). The authors are grateful for DONG Energy for the wind and wave measurements from Horns Rev and the EU Mermaid project for the FINO 1 wave data.

References

[1] Aarnes OJ, Breivik O, Reistad M. Wave extremes in the northeast atlantic. J Clim 2012;(25):1529–43.
[2] Abild J. Application of the wind atlas method to extremes of wind climatology. Roskilde, Denmark: Tech. Rep. Risoe-R-722(EN), Risø National Laboratory; 1994.
[3] Albers S. The LAP wind analysis. Weather Forecast 1995;10:342–52.
[4] Albers S, McGinley J, Birkerheuer D, Smart J. The local analysis and prediction system (LAPS): analysis of clouds, precipitation and temperature. Weather Forecast 1996;11:273–87.
[5] Behrens A, Günther H. Operational wave prediction of extreme storms in Northern Europe. Nat Hazards 2009;49:387–99.
[6] Bidlot J. Present status of wave forecasting at ECMWF. Tech. Rep. Proceedings from the ECMWF workshop on ocean waves, ECMWF. Reading: United Kingdom; 2012.
[7] Bidlot J, Janssen P. Unresolved bathymetry, neutral winds and new stress tables in WAM. Tech. Rep. ECMWF Research Department Memo R60.9/JB/0400, ECMWF. 2003.
[8] Bidlot J, Janssen P, Abdalla S, Hersbach H. A revised formulation of ocean wave dissipation and its model impact. Tech. Rep. ECMWF Tech. Memo 509, ECMWF. Reading: United Kingdom; 2007. p. 27. http://www.ecmwf.int/publications/.
[9] Bolaños-Sanchez R, Sanchez-Arcilla A, Cateura J. Evaluation of two atmospheric models for wind-wave modeling in the NW Mediterranean. J Mar Syst 2007;65:336–53.
[10] Cañellas B, Orfila A, Méndez F, Menéndez M, g.-P. L, Tintoré J. Application of a POT model to estimate the extreme significant wave height levels around the balearic sea (western mediterranean). J Coast Res 2007;(50):329–33.
[11] Caires S, Sterl A. 100-year return value estimates for ocean wind speed and significant wave height from the ERA-40 data. J Clim 2005a;18:1032–48.
[12] Caires S, Sterl A. A new nonparametric method to correct model data: application to significant wave height from the ERA-40 reanalysis. J Atmos Ocean Technol 2005b;22:443–59.
[13] Cavaleri L. Wave modeling - missing the peaks. J Phys Oceanogr 2009:2757–78.
[14] Cieslikiewicz W, Paplinska-Swerpel B. A 44-year hindcast of wind wave fields over the Baltic Sea. Coast Eng 2008;55:894–905.
[15] Emmanouil G, Galanis G, Kallos G, Breivik L, Heilberg H, Reistad M. Assimilation of radar altimeter data in numerical wave models: an impact study in two different wave climate regions. Ann Geophys 2007;25:581–95.
[16] Ferreira JA, Soares G. An application of the peaks over threshold method to periodic extremes of significant wave height. J Offshore Mech Arct Eng 1998;120:165–76.
[17] Galanis G, Emmanouil G, Kallos G, Chu P. A new methodology for extension of the impact in sea wave assimilation systems. Ocean Dyn 2009;59(3):523–35.
[18] Gumbel EJ. Statistics of extremes. Columbia University Press; 1958.
[19] Hasselmann S, Hasselmann K, Bauer E, Bertotti L, Cardone C, Ewing J, et al. The WAM model - a third generation ocean wave prediction model. J Phys Oceanogr 1988;18:1775–810.
[20] Hosking J. Estimation of the generalized extreme value distribution by the method of probability-weighted moments. Technometrics 1985;27:251–61.
[21] Janjic ZI. Nonlinear advection schemes and energy cascade on semi-staggered grids. Mon Weather Rev 1984;112:381–93.
[22] Janssen P. ECMWF wave modeling and satellite altimeter wave data. Elsevier; 2000.
[23] Janssen P, Lionello P, Reistad M, Hollingsworth A. A study of the deasibility of using sea and wind information from the ers-1 satellite, part 2: use of scatterometer and altimeter data in wave modeling and assimilation. Tech. rep., ECMWF. Reading, UK: eCMWF report to ESA; 1987.
[24] Janssen P, Onorato M. The intermediate water depth limit of the zakharov equation and consequences for wave prediction. J Phys Oceanogr 2007;37:2389–400.
[25] Johnson HK, Vested H, Hersbach H, Højstrup J, Larsen S. The coupling between wind and waves in the WAM model. J Atmos Ocean Technol 1999;16:1780–90.
[26] Kallos G. The regional weather forecasting system SKIRON. In: Proceedings, symposium on regional weather prediction on parallel computer environment, 15–17 Oct. 1997, Athens, Greece; 1997. p. 9.
[27] Kalnay E. Atmospheric modeling, data assimilation and predictability. Cambridge University Press; 2002.
[28] Kite GW. Confidence limits for design events. Water Resour Res 1975;11:48–53.
[29] Komen G, Cavaleri L, Donelan M, Hasselmann K, Hasselmann S, Janssen P. Dynamics and modeling of ocean waves. Cambridge University Press; 1994.
[30] Larsén XG, Mann J, Rathmann O, Jørgensen HE. Uncertainties of the 50-year wind from short time series using generalized extreme value distribution and generalized pareto distribution. Wind Energy 2015;18:59–74.
[31] Larsén XG, Ott S, Badger J, Hahmann AH, Mann J. Recipes for correcting the impact of effective mesoscale resolution on the estimation of extreme winds. J Appl Meteorol Clim 2012;51(3):521–33.
[32] Larsén XG, Vincent CL, Larsen S. Spectral structure of the mesoscale winds over the water. Q J R Meteorol Soc 2013;139:685–700.
[33] Leon SP, Soares G. Extreme wave parameters under North Atlantic extratropical hurricanes. Ocean Model 2014;81:78–88.
[34] Lionello P, Günther H, Janssen P. Assimilation of altermeter data in a global third generation wave model. J Geophys Res 1992;97(C9):14453–74.
[35] Magnusson L, Thorpe A, Bonavita M, Lang S, McNally T, Wedi N. Evalution of forecasts for hurricane Sandy. Reading: United Kingdom; 2013. Tech. Rep. ECMWF Tech. Memo 699, ECMWF.
[36] Mann J, Kristensen L, Jensen NO. Uncertainties of extreme winds, spectra and coherences. In: Larsen, Esdahl, editors. Bridge aerodynamics. Rotterdam: Balkema; 1998. ISBN 9054109610.
[37] Mesinger F. A blocking technique for representation of mountains in atmospheric models. Riv Meteorol Aeronaut 1984;44:195–202.
[38] Onorato M, Osborne A, Serio M, Cavaleri L, Brandini C, Stansberg CT. Observation of strongly non-gaussian statistics for random sea surface gravity waves in wave flume experiments. Phys Rev 2004;70:067302.
[39] Pilar P, Soares CG, Carretero J. 44-year wave hindcast for the North East Atlantic European coast. Coast Eng 2008;55:861–71.
[40] Ratsimandresey A, Sotillo M, Albiach JC, Álvarez Fanjul E, Hajji H. A 44-year high-resolution ocean and atmospheric hindcast for the Mediterranean basin developed within the HIPOCAS Project. Coast Eng 2008;55:827–42.
[41] Rugbjerg M, Sørensen OR, Jacobsen V. Wave forecasting for offshore wind farms. In: 9th International workshop on wave hindcasting and forecasting, Victoria, B.C. Canada, September 24–29; 2006.

[42] Rusu L, Soares G. Local data assimilation scheme to improve the wave predictions close to the portuguese ports. J Operational Oceanogr 2014;7:45–55.
[43] Saint-Drenan Y. Comparison of different charnock models for the determination of the vertical wind profile. Tech. rep., Fraunhofer Institut für Windenergie und Energiesystemtechnik IWES, RD Division Energy Economy and Grid Operation, Königstor 59, 34119 Kassel, Germany. 2009. http://www.hrensemble.net/public/pdf/HRensembleHR20091221IWES.pdf.
[44] Senet C, Fischer J, Outzen O, Herklotz K, Klein H. Remote sensing and in situ sea state instrument comparisons at the research platform FINO 1 in the German bight. geoscience and remote sensing symposium (IGARSS). IEEE Int 2012:7625–8. http://dx.doi.org/10.1109/IGARSS.2012.6351862. ISSN 2153-6996.
[45] Soares G, Cherneva Z, Petrova P, Antao E. Large waves in sea states in marine technology and engineering. London, UK: Taylor & Francis Group; 2011.
[46] Sommer A. Wind resources at horns rev. Tech. rep., Tech-wise A/S, report D-160949, available online at:. 2002. http://130.226.56.153/rispubl/NEI/nei-dk-4851.pdf.
[47] Sterl A, Caires S. Climatology, variability and extrema of ocean waves: the web-based KNMI/ERA-40 wave atlas. Int J Climatol 2005;25:963–77.
[48] Strauss D, Mirferendesk H, Tomlinson R. Comparison of two wave models for gold coast, Australia. J Coast Res 2007;(50):312–6.
[49] The-WISE-group. Wave modeling - the state of the art. Prog Oceanogr 2007;75:603–74.
[50] Vinoth J, Young I. Global estimates of extreme wind speed and wave height. J Clim 2011;24:1647–65.
[51] Wimmer W, Challenor P, Retzler C. Extreme wave heights in the North Atlantic from altimeter data. Renew Energy 2006;31:241–8.